Site-specific equilibrium isotopic fractionation of oxygen, carbon and calcium in apatite

Julie Aufort, Loïc Ségalen, Christel Gervais, Lorenzo Paulatto, Marc Blanchard, Etienne Balan

Available online at www.sciencedirect.com

ScienceDirect

Geochimica et Cosmochimica Acta 219 (2017) 57–73

Geochimica et Cosmochimica Acta

www.elsevier.com/locate/gca

Site-specific equilibrium isotopic fractionation of oxygen, carbon and calcium in apatite

Julie Aufort [a,*], Loïc Ségalen [b], Christel Gervais [c], Lorenzo Paulatto [a], Marc Blanchard [d], Etienne Balan [a]

[a] *Sorbonne Université, UPMC Université Paris 06 – Institut de Minéralogie, de Physique des Matériaux et de Cosmochimie (IMPMC), UMR CNRS 7590, UMR IRD 206, MNHN, 4 place Jussieu, 75252 Paris cedex 05, France*

[b] *Sorbonne Université, UPMC Université Paris 06 – Institut des Sciences de la Terre de Paris (ISTEP), Biominéralisations et Environnements Sédimentaires, UMR 7193, 4 place Jussieu, 75252 Paris cedex 05, France*

[c] *Sorbonne Université, UPMC Université Paris 06 – Laboratoire de Chimie de la Matière Condensée de Paris (LCMCP), UMR 7574, Collège de France, 4 place Jussieu, 75252 Paris cedex 05, France*

[d] *Géosciences Environnement Toulouse, Observatoire Midi-Pyrénées, CNRS-Université de Toulouse, 14, avenue Edouard Belin, 31400 Toulouse, France*

Received 19 December 2016; accepted in revised form 10 September 2017; Available online 19 September 2017

Abstract

The stable isotope composition of biogenic apatite is an important geochemical marker that can record environmental parameters and is widely used to infer past climates, biomineralization processes, dietary preferences and habitat of vertebrates. In this study, theoretical equilibrium isotopic fractionation of oxygen, carbon and calcium in hydroxyapatite and carbonate-bearing hydroxyapatite is investigated using first-principles methods based on density-functional theory and compared to the theoretical isotopic fractionation properties of calcite, CO_2 and H_2O. Considering the variability of apatite crystal-chemistry, special attention is given to specific contributions of crystal sites to isotopic fractionation. Significant internal fractionation is calculated for oxygen and carbon isotopes in CO_3 between the different structural sites occupied by carbonate groups in apatite (typically 7‰ for both $^{18}O/^{16}O$ and $^{13}C/^{12}C$ fractionation at 37 °C). Compared with calcite-water oxygen isotope fractionation, occurrence of A-type substitution in apatite structure, in addition to the main B-type substitution, could explain the larger temperature dependence of oxygen isotope fractionation measured at low temperature between carbonate in apatite and water. Theoretical internal fractionation of oxygen isotopes between carbonate and phosphate in B-type carbonated apatite (~8‰ at 37 °C) is consistent with experimental values obtained from modern and well-preserved fossil bio-apatites. Concerning calcium, theoretical results suggest a small fractionation between apatite and calcite (−0.17‰ at 37 °C). Internal fractionation reaching 0.8‰ at 37 °C occurs between the two Ca sites in hydroxyapatite. Furthermore, the Ca isotopic fractionation properties of apatite are affected by the occurrence of carbonate groups, which could contribute to the variability observed on natural samples. Owing to the complexity of apatite crystal-chemistry and in light of the theoretical results, measurements of site-specific isotopic fractionation properties could improve our understanding and the interpretation of isotopic records in apatites.

Keywords: Apatite; Ab initio; Stable isotope; Isotopic fractionation; Carbonate

* Corresponding author.
E-mail address: julie.aufort@impmc.upmc.fr (J. Aufort).

https://doi.org/10.1016/j.gca.2017.09.020
0016-7037/

1. INTRODUCTION

Apatite ($Ca_5(PO_4)_3X$, X = OH, F, Cl) is the most common phosphate mineral (McConell, 1973). It frequently contains minor amounts of carbonate, occurring naturally in substitution of phosphate (B site) and channel ions (A site) in the crystal structure (e.g. Fleet, 2009). While sedimentary deposits of carbonated fluorapatite yield the world's major phosphorus resources (Knudsen and Gunter, 2002), carbonated hydroxyapatite is the major inorganic component of vertebrate skeletons (Elliott, 2002). Stable isotope compositions of biogenic apatites, and in particular the isotope composition ($\delta^{13}C$, $\delta^{18}O$) of structural carbonate groups, are widely used to reconstruct past climates, past environments and dietary preferences of vertebrates (e.g. Kohn and Cerling, 2002; Roche et al., 2010; Roche et al., 2013; Pack et al., 2013; Reynard and Balter, 2014). For example, the carbon stable isotope composition of carbonate-bearing bio-apatites reflects that of ingested food and is used to infer dietary preferences of vertebrates in a variety of paleoecological studies (Lee-Thorp and van der Merwe, 1987; Quade et al., 1992). More recently, carbonate clumped isotopes (i.e. Δ_{47}) have generated a great interest (e.g. Schauble et al., 2006; Stolper and Eiler, 2015; Wacker et al., 2016) for their use as a geothermometer tool revealing formation temperatures of carbonate bearing minerals and, in particular, body temperature of vertebrates. The stable oxygen isotope composition of bioapatite is linked to the body water which depends on climatic and ecophysiological factors (Longinelli, 1984; Kohn et al., 1996). Beyond $\delta^{18}O$ measurements, high-precision triple oxygen isotope analysis (i.e. $\Delta^{17}O$) of carbonate minerals and structural carbonate in bioapatites is now also used to reconstruct past water compositions and has been suggested as a possible tracer for diagenetic alteration of fossil bones and teeth (Gehler et al., 2011; Passey et al., 2014).

Beside traditional isotopes, recent analytical advances have allowed the rapid development of Ca stable isotope composition analysis on bioapatites. Skulan et al. (1997) first reported the importance of biological calcium isotopic fractionation within the global calcium geochemical cycle and the possibility of calcium isotopic composition of fossils to record information on diet and environment. Calcium isotope fractionation in carbonate minerals has been widely investigated (Lemarchand et al., 2004; Marriott et al., 2004; Gussone et al., 2005). Several studies investigated carbonated bioapatites (Skulan and DePaolo, 1999; Heuser et al., 2009, 2011; Reynard et al., 2010; Tacail et al., 2016), providing reference values for $\delta^{44}Ca$ in biogenic apatite. Though marine carbonate sediments are the phase most commonly used for the reconstruction of calcium isotopic composition of seawater through time (Skulan et al., 1997; De La Rocha and DePaolo, 2000), the possibility of using other proxies such as foraminifera (Heuser et al., 2005) and phosphorites (Soudry et al., 2004) has been explored. Soudry et al. (2006) investigated the use of carbonated fluorapatite formed in marine sediments as a potential candidate for long term reconstructions of isotopic composition of seawater Ca^{2+}. Farkas et al. (2007) compiled records from various biogenic carbonates and authigenic phosphates to discuss the calcium isotope budget over Phanerozoic times. Calcium isotope fractionation might however vary depending on the type of phosphate deposit, e.g. sedimentary peloidal phosphates or phosphorite crusts (Arning et al., 2009). Considering the importance of understanding the oceanic mass balance of calcium and its impact on the regulation of carbon dioxide concentration in the atmosphere, the potentiality for calcium phosphate too to be used as a proxy for investigating past changes in Ca fluxes has to be determined. Despite this growing interest, the mechanisms and magnitude of calcium isotopic fractionation are still under debate.

The oxygen isotopic composition of biogenic apatite can also provide important information on paleotemperatures, its interpretation relying on the knowledge of apatite isotopic fractionation properties. Since the pioneering empirical studies of Longinelli (1965) and Kolodny et al. (1983), several experimental oxygen isotope fractionation relations have been established between bioapatite phosphate and water (Pucéat et al., 2010) and between dissolved phosphate and water (Chang and Blake, 2015). In low temperature systems the isotopic equilibrium cannot be achieved through efficient diffusion-mediated exchange between the relevant phases. In the case of phosphate, inorganic processes are not efficient enough to drive the system to equilibrium (Lécuyer et al., 1999). However it has been shown that enzymatic catalysis either related to microbial activity or intracellular metabolism enhances oxygen exchange between phosphate groups and water and could account for equilibrium exchange and temperature dependence observed in bioapatites and sedimentary apatites (Blake et al., 2005; Chang and Blake, 2015). An equation for oxygen isotope fractionation between carbonate groups in carbonated hydroxyapatite and water has also been determined from controlled experiments (Lécuyer et al., 2010). Uncertainties remain however, due to possible out-of-equilibrium isotope fractionation during crystal growth, slow isotope exchange rates and the variability of the apatite crystal-chemistry (Rakovan and Pasteris, 2015). Additional difficulties may also arise when non-conventional stable isotopes are investigated due to the small magnitude of isotopic fractionation factors (e.g. Blanchard et al., 2017). Experimental equilibrium fractionation laws may therefore be affected by large uncertainties at low temperatures.

Alternatively, equilibrium fractionation factors can be determined theoretically from the computation of vibrational properties. The advantages of calculating fractionation factors within first principles methods are to provide independent equilibrium fractionation laws, over a wide range of temperatures, from which comparison with experimental data may help understand deviations from equilibrium values and kinetic effects. Theoretical computation of isotopic fractionation properties can also be applied to non-conventional isotopes for which experimental measurements are difficult or lacking. A variety of isotopes and minerals have been investigated using first-principles methods based on density functional theory (DFT), such as stable isotopes O and C in carbonates (Schauble et al.,

2006), and H, O and Si in silicates (Méheut et al., 2007). Theoretical studies of calcium isotopic fractionation have also been conducted on sulfates (Griffith et al., 2008) and carbonates (Rustad et al., 2010; Wang et al., 2017). In addition, theoretical approaches make it possible to determine the isotopic fractionation properties of specific sites in the crystal structure (e.g. Méheut et al., 2007; Rustad and Zarzycki, 2008; Zheng, 2016).

The aim of the present study is to provide a theoretical framework for equilibrium isotopic fractionation in apatite and to assess possible isotopic fractionation arising from carbonate substitution in different sites of the apatite crystal lattice. Isotopic fractionation properties of apatite are compared to that of other phases of interest in order to discuss a variety of geochemical contexts. In this work, we use the same first-principles approach as Méheut et al. (2007) to determine the stable isotopic fractionation of oxygen, carbon and calcium in the hydroxyapatite, calcite, water and CO_2 system. In addition, the equilibrium isotopic fractionation properties of three energy-minimized theoretical models for carbonate substitution in apatite whose structural and vibrational properties were discussed in Yi et al. (2014) are also investigated.

2. METHODS

2.1. Equilibrium isotopic fractionation factors

The equilibrium isotopic fractionation factor $\alpha(a, b, Y)$ of an element Y between two phases a and b is defined as the ratio of isotope ratios (atomic fraction) in phase a compared to phase b. It can also be written as the ratio of the reduced partition function ratios:

$$\alpha(a, b, Y) = \frac{\beta(a, Y)}{\beta(b, Y)} \tag{1}$$

where $\beta(a, Y)$ is the reduced partition function ratio of phase a. This β-factor can be seen as the equilibrium isotope fractionation factor between phase a and a perfect gas of Y atoms. The reduced partition function ratio can be calculated from the harmonic vibrational frequencies (Bigeleisen and Mayer, 1947) as follows:

$$\beta(a, Y) = \left[\prod_{i=1}^{3N_{at}} \prod_{\{\boldsymbol{q}\}} \frac{\nu_{\boldsymbol{q},i}}{\nu'_{\boldsymbol{q},i}} \frac{\exp(-h\nu_{\boldsymbol{q},i}/2k_BT)}{1-\exp(-h\nu_{\boldsymbol{q},i}/k_BT)} \frac{1-\exp(-h\nu'_{\boldsymbol{q},i}/k_BT)}{\exp(-h\nu'_{\boldsymbol{q},i}/2k_BT)}\right]^{1/(N_qN)} \tag{2}$$

where $\nu_{\boldsymbol{q},i}$ and $\nu'_{\boldsymbol{q},i}$ are the phonon frequencies of the two isotopologues (the prime symbol refers to the light isotope of the element Y) identified by a wavevector $\boldsymbol{q}$ and a branch index $i = 1, 3N_{at}$. N_{at} is the number of atoms in the crystal unit cell, h is the Planck's constant, k_B Boltzmann's constant and T the temperature. The second product is performed on a sufficiently large grid of N_q $\boldsymbol{q}$-vectors in the Brillouin zone. In Eq. (2) the three translational modes with $\nu_{\boldsymbol{q},i} = 0$ are not considered. N is the number of exchanged sites for the Y element in the unit cell. Eq. (2) takes into account the Teller-Redlich rule (Redlich, 1935) which imposes $\lim_{T\to\infty}\beta = 1$.

2.2. Modelling approach and density-functional theory calculations

The phonon frequencies necessary to calculate the reduced partition function ratios (Eq. (2)) are computed from first-principles methods within density functional theory (DFT) (Hohenberg and Kohn, 1964; Kohn and Sham, 1965). All calculations reported here are performed with the generalized-gradient approximation (GGA) for the exchange-correlation functional as proposed by Perdew, Burke and Ernzerhof, abbreviated PBE (Perdew et al., 1996). The structural and vibrational calculations are performed using the PWscf and PHonon codes of the Quantum Espresso package (Giannozzi et al., 2009). The ionic cores of Ca, P, O, F, C, and H are described by optimized norm-conserving Vanderbilt (ONCV) pseudopotentials (Hamann, 2013). Electronic wave functions and charge density are expanded in plane waves using 80 Ry and 800 Ry cut-offs respectively so that total energies are converged within 1 mRy/atom. Electronic integration is performed by sampling the Brillouin zone with a $2 \times 2 \times 2$ k-points grid for hydroxyapatite and a $3 \times 3 \times 3$ k-point grid for calcite according to the Monkhorst and Pack (1976) scheme. Atomic positions are obtained after relaxation until the residual forces are less than 10^{-4} Ry/au. For the pure crystal phases, the residual pressure over the relaxed cell is smaller than 0.02 kbar.

The lattice parameters of DFT relaxed structures of hydroxyapatite and calcite compare well with their experimental counterparts (Table 1) and previous theoretical modelling at the PBE level (Balan et al., 2011). In both cases, calculated lattice parameters are overestimated by ~1%, which is a systematic error in density functional theory calculations performed using GGA PBE functionals. Models of carbonated apatite have been built, starting from defect structures previously obtained by Yi et al. (2014). In the present study, B-type carbonated hydroxyapatite ($Ca_{10}(PO_4)_5(CO_3F)(OH)_2$) and A-type carbonated apatite ($Ca_{10}(PO_4)_6(CO_3)$) were considered. To test the chemical effect of F^- ions located in channel sites, an additional B-type model was also considered by exchanging F^- ions for the channel OH groups, leading to a carbonated-fluorapatite composition ($Ca_{10}(PO_4)_5(CO_3F)F_2$). For all these models, the atomic positions were optimized while the cell parameters were kept fixed to those of pure hydroxyapatite (constant-volume relaxation) and using a $2 \times 2 \times 2$ k-points grid. Note that only a direct chemical

Table 1
Hydroxyapatite and calcite calculated and experimental lattice parameters.

Hydroxyapatite	This work	Exp[a]
a (Å)	9.567	9.417
c (Å)	6.890	6.875
Calcite	**This work**	**Exp[b]**
a (Å)	6.444	6.375
γ (°)	46.03	46.08

[a] Hughes et al. (1989).
[b] Graf (1961).

effect of channel fluorine on the carbonate models was tested whereas the reduction of the cell volume observed in pure fluorapatite with respect to hydroxyapatite was not considered in the present study. A cubic cell ($a = 15.87$ Å) was used to build periodic models of isolated H_2O and CO_2 molecules. In addition, a periodic model of the isolated $[Ca(H_2O)_6]^{2+}$ molecule was also calculated using the same cubic cell to benchmark our calcium isotopic fractionation calculations. In these cases, the Brillouin zone sampling for the electronic integration is restricted to the Γ-point.

Phonon frequencies are computed using density functional perturbation theory (DFPT) (Baroni et al., 2001). Interatomic force constants are obtained from the dynamical matrices first computed exactly within DFPT on a regular $m \times m \times m$ grid of **q**-vectors ($m = 3$ for calcite and hydroxyapatite). Vibrational frequencies for the two isotopologues are then obtained by diagonalising the dynamical matrices computed with the two different atomic masses on a $n \times n \times n$ grid obtained by Fourier interpolation of the interatomic force constants. The vibrational partition function is converged by performing the product on a $3 \times 3 \times 3$ grid for hydroxyapatite and $4 \times 4 \times 4$ for calcite (Table S1). For the models of carbonate bearing apatites, phonon frequencies, and related β-factors, were obtained at the centre of the Brillouin zone only (Γ point). The results will be discussed in terms of logarithmic β-factors, ln (β), and logarithmic fractionation factors, ln (α), expressed in parts per thousands (‰). Polynomial fits of the β-factors are reported in Table S3.

The comparison between theoretical and actual equilibrium isotopic fractionation factors is affected by the various assumptions and approximations used in the modelling approach. As previously discussed by Méheut et al. (2007, 2009) and Dupuis et al. (2015), theoretical reduced partition function ratios are systematically affected by the choice of the functional used to compute the electronic structure of the system (here the PBE functional) and the neglect of anharmonic effects. The theoretical frequencies computed at the centre of the Brillouin zone of crystals can be compared to their experimental counterparts (Table S2). An overall ~5% underestimation of calculated phonon frequencies is observed, a systematic error associated with the overestimation of lattice parameters seen in DFT calculations performed with a PBE approximation (Favot and Dal Corso, 1999). Such underestimation is expected to lead to a relative underestimation of logarithmic β-factors ranging between −5 and −10% (Méheut et al., 2007, 2009). In order to correct the systematic errors encountered with PBE approximation, a uniform scaling of the calculated PBE frequencies could be used to match the experimental ones (e.g. Schauble et al., 2006). This approach however depends on the availability and accuracy of spectroscopic data recorded on molecular and crystalline systems, potentially introducing additional uncertainties. For this reason, it was not used in the present study. The β-factors were obtained solely from the raw theoretical harmonic frequencies computed within DFT.

A different source of uncertainty affecting the comparison of the theoretical data and experimental measurements arises from the strategy used to model the carbonate defects in the apatite crystal host. Although the theoretical carbonate concentration (~4.4 wt% of CO_2) is consistent with the concentrations observed in biogenic samples (4.8 wt% of CO_2 in bone, Elliott, 2002), the periodic models do not account for the random character of substitutions affecting equivalent sites in minerals. A relaxation of the cell-parameters of the defect model would prejudicially increase this character by constraining the full system symmetry to that locally imposed by the defect. A theoretical relaxation of atomic positions using experimental cell-parameters would also introduce an unconstrained inconsistency in the model. In the present study, all the defect models were thus built by keeping the cell parameters identical to that of pure hydroxyapatite. Sensitivity tests were however performed on the A and B carbonate models using an isotropic relative contraction of the cell parameters of 0.7% (corresponding to the relaxed volume of the defects models). They lead to 1.5‰, 0.8‰ and 0.8‰ increases in oxygen, carbon and calcium β-factors at 300 K, respectively. For the models of carbonate bearing apatites, oxygen, carbon and calcium β-factors were also determined from phonon frequencies calculated at the special point of the hexagonal lattice (Chadi and Cohen, 1973). They are systematically higher by 0.5‰, 0.4‰ and 0.35‰ at 300 K respectively, in all carbonate-bearing apatites, than β-factors determined from phonon frequencies calculated at the Γ point. Because these variations are consistent for all carbonated apatites, they would not alter the fractionation factors related to different schemes of carbonate incorporation in apatite.

3. RESULTS

3.1. Oxygen $^{18}O/^{16}O$ equilibrium fractionation properties

For the investigated phases, oxygen β-factors at 25 °C vary from 60‰ to 110‰ (Fig. 1a). This significant variability is mostly due to the different nature of bonds with covalent character involving oxygen in these phases (O-H, P-O and C-O), which leads to differences in interatomic force constants. In the case of hydroxyapatite, oxygen atoms are either bound to phosphorus atoms or hydrogen atoms, a different behaviour regarding isotopic fractionation is therefore expected between phosphate and hydroxyl sites. Site-specific oxygen β-factors in hydroxyapatite were computed by either substituting the oxygen atoms belonging to hydroxyl groups (OH), or the oxygen atoms belonging to phosphate groups (PO_4), or both (Table S3).

At equilibrium, phosphate oxygens are enriched in ^{18}O relative to hydroxyl oxygens (Fig. 1b) and the phosphate oxygen β-factor is close to the total oxygen β-factor in hydroxyapatite. Nearly all the fractionation takes place in the internal vibration of the PO_4 tetrahedron, with ν_2, ν_4, ν_1 and ν_3 PO_4 modes contributing to about 8‰, 15‰, 13‰ and 30‰ respectively. Smaller β-factors are observed for OH-groups compared to total oxygen β-factors (Table 2). The oxygen β-factor of hydroxyl groups is dominated by their stretching mode (Fig. 2a). Overall, the OH groups only weakly contribute to the total oxygen β-factor of hydroxyapatite, with 0.97‰ and 0.07‰ respectively.

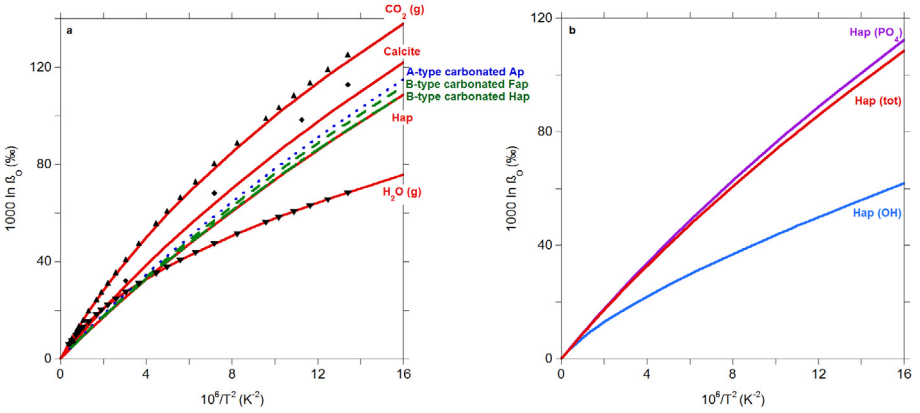

Fig. 1. (a) Oxygen isotope β-factors for: gas H_2O (isolated molecule), gas CO_2 (isolated molecule), calcite, hydroxyapatite, and three theoretical models for carbonate substitution in apatite: B-type carbonated fluorapatite (as proposed by Yi et al. (2013)) $Ca_{10}(PO_4)_5(CO_3F)F_2$, B-type carbonated hydroxyapatite $Ca_{10}(PO_4)_5(CO_3F)(OH)_2$ and A-type carbonated apatite ($Ca_{10}(PO_4)_6(CO_3)$). Oxygen β-factors of calcite (solid diamonds) determined using DFT calculations performed by Schauble et al. (2006), and CO_2 and H_2O (open upwards and downwards triangles respectively) calculated using experimental molecular constants and anharmonic calculations by Richet et al. (1977). (b) Oxygen β-factors for hydroxyapatite (OH): oxygen atoms belonging to a hydroxyl group in hydroxyapatite, hydroxyapatite (PO_4): oxygen atoms belonging to a phosphate group, hydroxyapatite (tot): total oxygen β-factor in hydroxyapatite.

Table 2
Logarithm of site-specific oxygen β-factors (‰) for hydroxyapatite, B-type carbonated hydroxyapatite, B-type carbonated fluorapatite and A-type carbonated apatite at T = 300 K.

1000 ln β	All O sites	PO_4 sites	OH sites	CO_3 sites
Hydroxyapatite	80.4056	83.1800	47.0975	–
B-type carbonated hydroxyapatite	80.6355	82.3141	48.7959	90.6614
B-type carbonated fluorapatite	83.0130	81.8706	–	90.6244
A-type carbonated apatite	85.1984	83.6017	–	97.9628

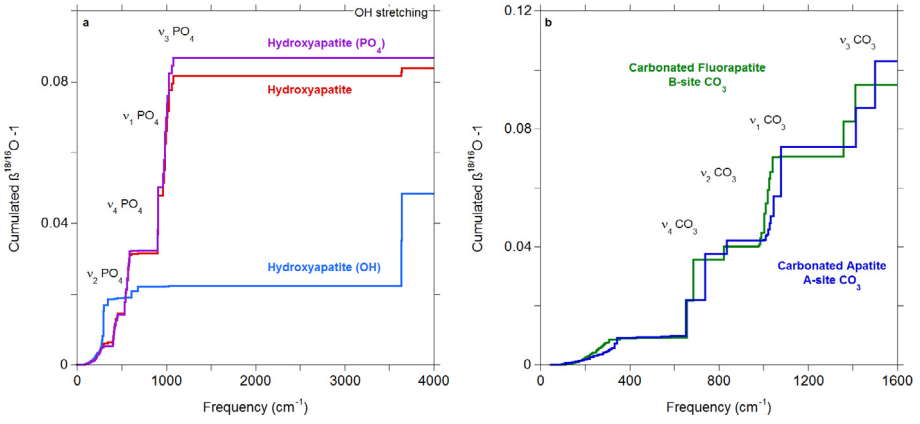

Fig. 2. (a) Cumulative contributions to the reduced partition function ratio (given as $\beta^{18/16}O - 1$, following the representation given by Rustad et al. (2010)), for $^{18/16}O$ in hydroxyapatite, hydroxyl (OH) and phosphate (PO_4) groups in Hap at 300 K. (b) Cumulative contributions to the reduced partition function ratio given as $\beta\ ^{18/16}O - 1$, for $^{18/16}O$ in carbonate sites in carbonated fluorapatite and carbonated apatite at 300 K.

Depletion in ^{18}O relative to calcite is observed for all oxygen sites in hydroxyapatite and carbonated apatite phases. Total oxygen β-factors in carbonate-bearing apatites (Fig. 1a) vary depending on the carbonate substitution site, with A-type carbonate substitution leading to enrichment in ^{18}O relative to B-type substitution. Site-specific oxygen β-factors were calculated for the three carbonate defect models and results are shown at 300 K in Table 2. Distinctive isotopic fractionation behaviours are observed from one oxygen site to another, depending on the type of atom, H, P or C, bound to oxygen (Table 2). The presence of B-type carbonate groups decreases the oxygen β-factors of structural phosphates by 0.9–1.3‰ at 300 K. In contrast, occurrence of A-type carbonate leads to a smaller increase of 0.4‰. Oxygen is heavier in structural carbonate of apatites than in phosphate, regardless of the substitution

site (A or B). However, the isotopic fractionation behaviour of oxygen in carbonate groups differs depending on the substitution site for carbonate in apatite. Carbonate substituted to hydroxyl (A-type) is richer in ^{18}O than is carbonate substituted to phosphate (B-type). The differences in oxygen fractionation between A-type and B-type substituted carbonate in apatites (Table 2) arise mainly from the ν_3 CO_3 mode (Fig. 2b). Other CO_3 modes contribute to about the same amount in both A-type and B-type carbonates whereas ν_3 contributes to 27‰ and 22‰ respectively, making up for ~70% of the enrichment in ^{18}O in A-type CO_3 relative to B-type (Fig. 2b). The differences observed among experimental vibrational spectra of B-type carbonate in hydroxyapatite, bioapatite, and sedimentary carbonate-rich fluorapatite (also known as 'francolite') are smaller than those observed between A-type and B-type carbonate spectra. The ν_2 CO_3 bending mode are observed at ~865 cm^{-1} in 'francolite' (Regnier et al., 1994; Fleet, 2009) and ~873 cm^{-1} for B-site carbonates, whereas the two anti-symmetric stretching ν_3 CO_3 modes correspond to relatively broad bands at ~1430 and ~1450 cm^{-1} and at ~1410 and ~1450 cm^{-1}, respectively (Yi et al., 2014b). The observed differences arise from a different charge compensation mechanism of the carbonate for phosphate substitution which involves a nearby fluoride ion in the 'francolite' defect (Yi et al., 2013). Accordingly, the carbonated fluorapatite model investigated in this work can be considered a good proxy for studying isotopic fractionation properties related to B-type carbonate in apatite.

At 25 °C the oxygen β-factor is 61.8‰ for the isolated H_2O molecule (Fig. 1a), this corresponds to a logarithmic difference of less than 1‰ with previous harmonic calculations based on DFT models (PBE functional; Méheut et al., 2007) or anharmonic calculation based on experimental molecular constants (Richet et al., 1977). In the case of water, harmonic frequencies calculated with the PBE functional are underestimated with respect to their experimental counterparts and almost coincide with the experimental (anharmonic) values (Table S2). A cancellation of errors (Balan et al., 2007), i.e. underestimation of the OH bonds harmonic frequencies in water and lack of anharmonicity in Eq. (2) fortuitously yields the good agreement observed between the calculated and experimental β-factors.

The oxygen β-factor of calcite is lower (by 6‰ at 25 °C) than that reported by Schauble et al. (2006). This is mostly due to the frequency scaling introduced by Schauble et al. (2006) to better match the experimentally measured frequencies. Our calculations for CO_2 differ from Richet et al. (1977) by ~2.5‰ at 25 °C (for a β-factor of ~110‰).

3.2. Carbon $^{13}C/^{12}C$ equilibrium fractionation properties

Carbon β-factor values are higher than oxygen β-factors and vary from 170 to 180‰ at 25 °C in the investigated phases, with smaller relative variations from one phase to the other than what was observed for oxygen fractionation (Fig. 3), reflecting that carbon only occurs as a carbonate group. As in the case of oxygen, the isotopic fractionation behaviour of carbon in carbonate groups differs depending on the substitution site, A or B, for carbonate in apatite. The occupation of the structural channels in B-type carbonated apatite by hydroxyl or fluoride ions has no effect on carbon β-factor as both curves are superimposed. Carbonate substituted to channel ions (A-type substitution) is enriched in the heavy isotope (^{13}C) compared to carbonate substituted for phosphate, with an 8‰ difference at 300 K. Unlike oxygen fractionation, carbon in calcite is lighter than that of CO_3 in A-type carbonated apatite at equilibrium.

3.3. Calcium $^{44}Ca/^{40}Ca$ equilibrium fractionation properties

Logarithmic values of calcium β-factors are one order of magnitude smaller than those of carbon and vary from 10.9 to 12.1‰ at 25 °C in the investigated phases (Fig. 4a). Values for calcite from theoretical calculations performed by Rustad et al. (2010) on molecular clusters are higher than our calculations by ~4‰ at 300 K. This is to be expected because the computational method is different, involving molecular clusters instead of crystal cell and the B3-LYP hybrid functional instead of PBE. For comparison, similar calculations of $[Ca(H_2O)_6]^{2+}$calcium β-factor at the PBE level lead to a 10.96‰ value at 37 °C, which is lower by 2.5‰ than the B3-LYP calculations of Moynier and Fujii (2017). This also shows that caution must be taken not to derive fractionation factors from β-factors computed with different parameters and methods when comparing with experimental measurements. Similarly to oxygen and carbon isotopic fractionation, calcium β-factors vary depending on the carbonate substitution site, with A-type carbonated apatite displaying the heaviest Ca isotopic composition.

With the growing interest in fossil bio-apatite calcium isotope composition for paleoenvironmental reconstructions, an increasing number of studies provide δ-Ca values, mainly $\delta^{44/40}Ca$ and $\delta^{44/42}Ca$. The mass difference for $^{44}Ca/^{40}Ca$ is double compared to $^{44}Ca/^{42}Ca$. The mass-dependent isotope fractionation ratio of the former should therefore be about twice the isotope ratio for the latter but the exact relationship between the two depends on the fractionation mechanism involved, equilibrium or kinetic. We calculated the factor between our theoretical $^{44/40}Ca$ and $^{44/42}Ca$ β-factors for calcite and hydroxyapatite. In both cases, a 2.10 factor ($\delta^{44/40}Ca = 2.10 \times \delta^{44/42}Ca$) is obtained from theoretical computation of calcium β-factors, identical to the equilibrium value previously obtained by Young et al. (2002) using the formula $\frac{1/m_{44_{Ca}} - 1/m_{40_{Ca}}}{1/m_{44_{Ca}} - 1/m_{42_{Ca}}}$. It differs from the 2.05 factor obtained for a kinetic isotope fractionation mechanism (Young et al., 2002; Gussone et al., 2016).

Calcium atoms in apatite exist in two coordination polyhedra (Hughes et al., 1989, 1990). Ca(I) resides at the centre of a trigonal prism involving 9 oxygen atoms whereas Ca (II) is bound to 6 oxygen atoms and one column anion (OH^-, F^-). Site-specific calcium isotopic fractionation was investigated (Fig. 4b) and shows that while Ca(II) is more susceptible to enrichment in heavy isotope in hydroxyapatite, the presence of carbonated groups affects the isotopic fractionation properties of nearby Ca sites. The Ca(II) is still heavier than Ca(I) in B-type carbonated

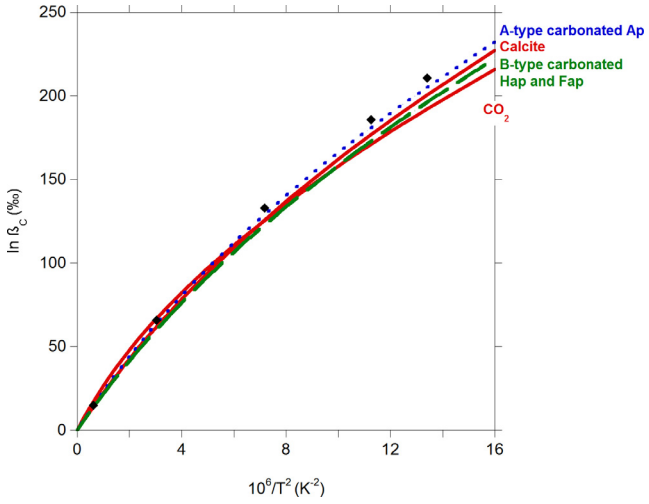

Fig. 3. Carbon isotope β-factors in calcite, B-type carbonated hydroxyapatite, B-type carbonated fluorapatite, A-type carbonated apatite and CO_2. Carbon β-factor of calcite (solid diamonds) determined using DFT calculations performed by Schauble et al. (2006).

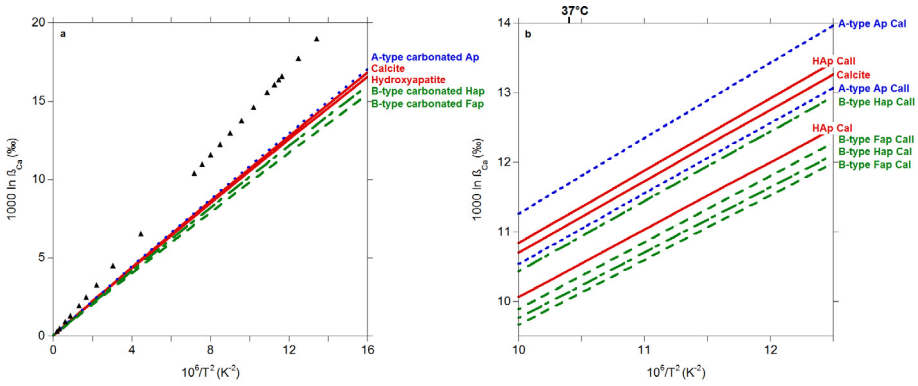

Fig. 4. (a) Calcium isotope ($^{44}Ca/^{40}Ca$) β-factors in calcite, hydroxyapatite, B-type carbonated fluorapatite, B-type carbonated hydroxyapatite and A-type carbonated apatite. Solid triangles correspond to calcite-type molecular cluster calculated using the B3-LYP functional (Rustad et al., 2010). (b) Calcium ($^{44}Ca/^{40}Ca$) β-factors in calcite and for Ca(I) and Ca(II) sites in hydroxyapatite, B-type carbonated fluorapatite, B-type carbonated hydroxyapatite and A-type carbonated apatite between 10 °C and 40 °C.

fluorapatite whereas A-type carbonate substitution leads to a preference of the Ca(I) sites for the heavy isotopes. From hydroxyapatite to B-type carbonated hydroxyapatite, the difference in β-factor between Ca(II) and Ca(I) remains about the same, with carbonate substitution lowering both values equally. Replacement of structural channel hydroxyls by fluoride ions reduces the difference between Ca(II) and Ca(I) by half.

4. DISCUSSION

4.1. Equilibrium isotopic fractionation of oxygen $^{18}O/^{16}O$

4.1.1. Carbon dioxide/liquid water oxygen isotope fractionation

As direct calculation of the reduced partition function ratio of liquid water is computationally very demanding (e.g. Pinilla et al., 2014), we used the same hybrid approach as Méheut et al. (2007) and calculated the CO_2/liquid water fractionation from the theoretical CO_2/water vapour fractionation and the experimental liquid/vapour fractionation for water determined by Horita and Wesolowski (1994). Theoretical oxygen isotopic fractionation between carbon dioxide and liquid water (Fig. 5) differs by ~3‰ from experimental measurements (Bottinga and Craig, 1969) and calculations from Richet et al. (1977) at 25 °C, an error arising from the ~2.5‰ lower theoretical β-factor value obtained for CO_2 (Fig. 1). The hybrid approach involving experimental liquid/vapour fractionation thus yields sound comparison between our calculations and experimental values, and the same approach was used to obtain oxygen fractionation between mineral phases and liquid water.

4.1.2. Mineral/liquid water oxygen isotope fractionation: calcite and structural phosphate in apatite

Two different empirical bio-apatite phosphate-water equations have been reported in the literature (Kolodny et al., 1983; Pucéat et al., 2010). The ~2‰ offset between the equation of Pucéat et al. (2010) and previous determination by Kolodny et al. (1983) is related to differences in

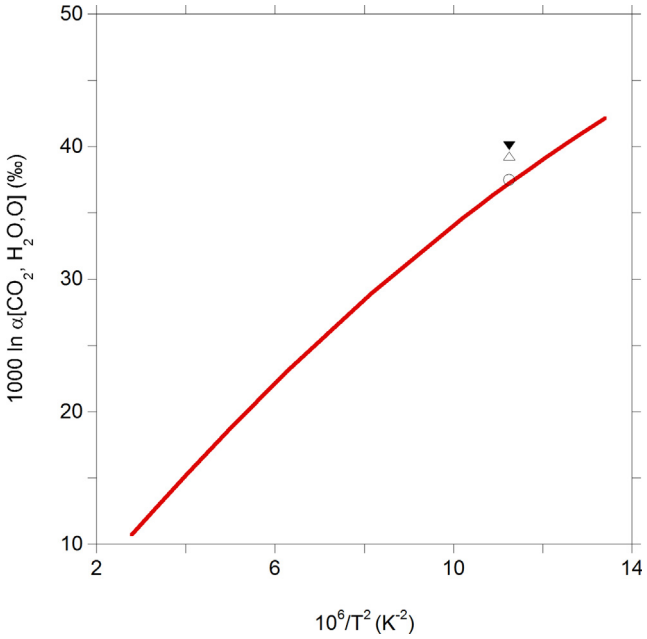

Fig. 5. Theoretical oxygen isotope fractionation factor between gaseous carbon dioxide and liquid water (solid line). Experimental oxygen fractionation factors measured by Bottinga and Craig 1969 (solid downward triangle). Oxygen fractionation factor between CO_2 and H_2O determined from β-factors calculated using experimental molecular constants and anharmonic calculations by Richet et al. (1977) (open upward triangle) and Urey (1947) (open circle) at 25 °C.

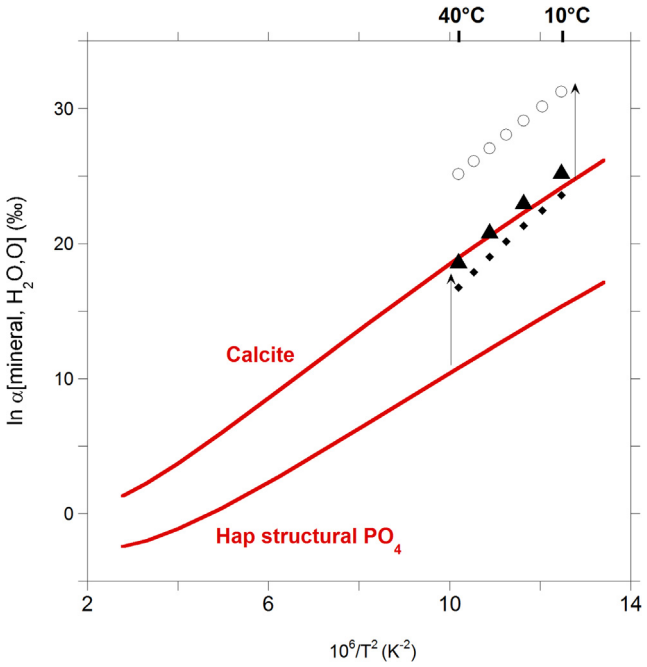

Fig. 6. Theoretical oxygen isotopic fractionation factor between calcite or hydroxyapatite phosphate (solid lines) and liquid water $H_2O(l)$ for temperatures below T_c, the critical temperature of liquid water. Experimental calcite-water equation (Kim and O'Neil, 1997) in open circles, phosphate-water equation from Kolodny et al. (1983) in solid diamonds and Pucéat et al. (2010) in solid triangles between 10 and 40 °C. Vertical arrows facilitate the visual comparison by pointing to the corresponding experimental values.

analytical methods (modern analysis of Ag_3PO_4 replaced fluorination of $BiPO_4$) and in values used for the NBS SRM 120c standard. The deviation observed between these equations and our calculation for hydroxyapatite phosphate – liquid water fractionation (~7‰ compared to Kolodny et al., 1983 and ~8.5‰ compared to Pucéat et al., 2010) is similar to that observed for the calcite-water fractionation (Fig. 6). Between 10 and 40 °C the

difference between calculation and measurements of oxygen isotope fractionation between calcite and liquid water (Kim and O'Neil, 1997) is about 6.5‰ (Fig. 6). This suggests that these differences are systematic and mostly related to the underestimation of frequencies of the vibrational modes in the solid phase calculated using the PBE functional. This sustains the model by which equilibrium between dissolved phosphate, apatite and water at low temperatures would be driven by catalytic mechanisms (Blake et al., 2005; Liang and Blake, 2007). Note that the fractionation between dissolved phosphate and apatite at low temperatures could also depend on the different dissolved phosphate species (e.g. $H_2PO_4^-$, HPO_4^{2-}) in solution with respect to pH. Zheng (2016) also calculated apatite phosphate – water fractionation using an increment method based on the correlation between bond strength and isotopic fractionation. The related values are however different since the assumptions made are not comparable with that of DFT calculations.

4.1.3. Oxygen isotope fractionation between structural carbonate in apatite and liquid water

The slope for experimental calcite – liquid water fractionation measured by Kim and O'Neil (1997) between 10 and 40 °C (Fig. 7a) is well reproduced by the theoretical calculations. An offset of 6.5‰ allows for the theoretical fractionation values to match the absolute experimental values (Fig. 7b). Oxygen isotope fractionation between B-type carbonated apatite and liquid water is close to that of calcite and water. The occupancy of the structural channels in B-type carbonated apatite by either OH^- or F^- ions does not affect the B-type carbonate/liquid water fractionation. Fractionation factors for A-type carbonated apatite are about 6‰ higher than those of B-type. As a result, both theoretical A-type carbonated apatite fractionation and experimental calcite-water fractionation curves seem to coincide but this is merely due to a compensation of the offset. If all theoretical fractionation curves are shifted by +6.5‰ so that theoretical and experimental calcite – liquid water fractionation curves coincide, a situation shown in Fig. 7b, theoretical B-type carbonated apatite – liquid water fractionation then matches very well the measurement of Lécuyer et al. (2010) at 40 °C. At 10 °C, however, the calculated equilibrium fractionation is then ~3‰ lower than the experimental value. Based on the equilibrium fractionation factors, we calculate that the equilibrium fractionation factor coinciding with the value of Lécuyer et al. (2010) at 10 °C can be obtained for a carbonate-bearing apatite with roughly one third A-type and two thirds B-type carbonates. At 20 °C the experimental value is matched for a carbonate-bearing apatite with one quarter A-type and three quarters B-type carbonates. Accordingly, a possible explanation for the steeper slope observed by Lécuyer et al. (2010) in comparison to other experimental carbonate/water equations (Kim and O'Neil, 1997) and our theoretical equation, could be the variation of the A/B carbonate ratio with temperature. Note that these A/B ratios are consistent with the dominant nature of B-type substitution in natural carbonate-bearing bioapatites.

4.1.4. Hydroxyapatite oxygen internal fractionation

Internal fractionation of oxygen isotopes between sites belonging to a hydroxyl group and sites belonging to a phosphate group was computed from site specific β-factors in hydroxyapatite and in B-site carbonated hydroxyapatite (Fig. 8). Note that some uncertainties of the theoretical models are expected to be more efficiently compensated when calculating internal fractionation factors (i.e. isotopic fractionation between two different sites in the same material). The theoretical fractionation between non hydroxyl and hydroxyl sites, 36.5‰ at 25 °C, is significantly more important in hydroxyapatite than in kaolinite, for which Méheut et al. (2007) calculated a 12‰ fractionation factor at 25 °C. In B-type carbonate-bearing models, phosphate is lighter than in non-carbonated hydroxyapatite, resulting in a smaller internal fractionation with hydroxyl (cf Table 2).

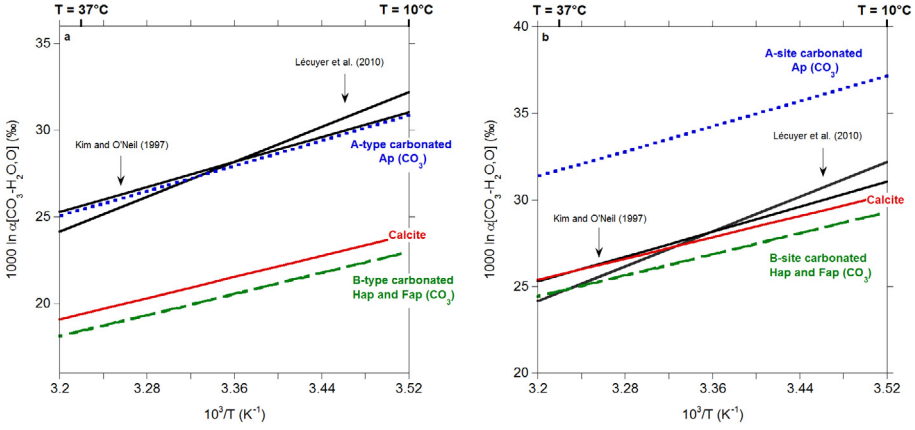

Fig. 7. (a) Theoretical oxygen isotopic fractionation factor between carbonate in calcite or in carbonate-bearing apatites and liquid water compared to experimental fractionation between inorganic hydroxyapatite carbonate and water (Lécuyer et al., 2010) and the inorganic calcite-water equation (Kim and O'Neil, 1997) in the range 10–40 °C. (b) Theoretical oxygen isotope fractionation curves between various apatite phases (A-type carbonated hydroxyapatite, B-type carbonated hydroxyapatite and B-type carbonated fluorapatite) and $H_2O_{(l)}$ shifted by +6.5‰.

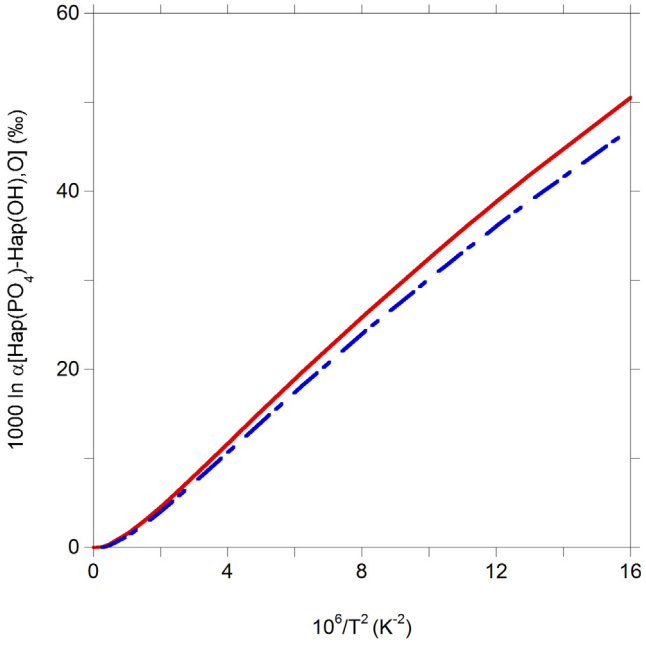

Fig. 8. Theoretical phosphate/hydroxyl oxygen intracrystalline fractionation factor in hydroxyapatite (solid line) and in B-type carbonated hydroxyapatite (dash-dot line).

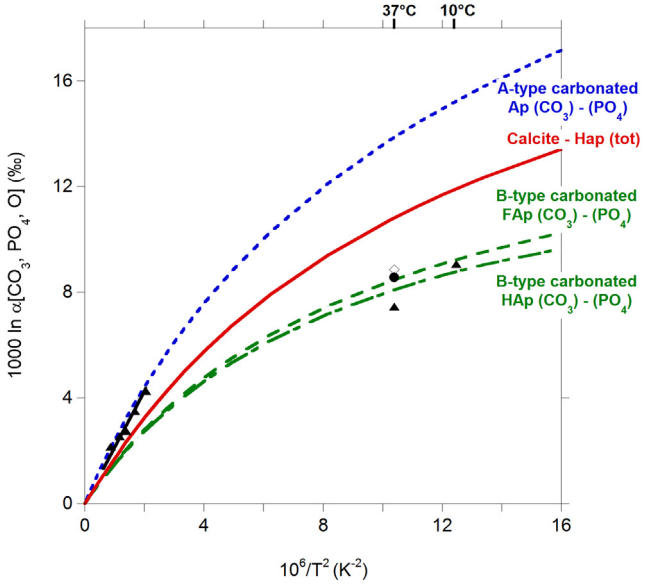

Fig. 9. Theoretical internal oxygen isotope fractionation factor between oxygen atoms belonging to carbonate sites only (CO_3) and oxygen atoms belonging to phosphate sites only (PO_4) in B-type carbonated fluorapatite (dashed line), in B-type carbonated hydroxyapatite (dash-dot line) and in A-type carbonated apatite (dotted line). Theoretical oxygen isotope fractionation factor between calcite and hydroxyapatite with all oxygen sites (OH and PO_4) taken into account. Experimental high temperature oxygen isotope fractionation between calcite and inorganic hydroxyapatite by Fortier and Lüttge (1995) (solid triangles) and linear regression through the origin of high temperature data from Fortier and Lüttge (1995) by Chacko et al. (2001) (black solid line). Experimental isotope fractionation factors between phosphate and structural carbonate determined from bone and tooth samples of modern mammals at 37 °C by Bryant et al. (1996) (solid circle) and Iacumin et al. (1996) (open diamond). Experimental isotope fractionation factors between phosphate and structural carbonate determined at 10 °C and 37 °C using carbonate values from Lécuyer et al. (2010) and phosphate values from Kolodny et al. (1983) (solid triangles).

4.1.5. Oxygen isotope fractionation between structural carbonates and phosphates in apatite

High temperature theoretical oxygen isotope fractionation between calcite and hydroxyapatite differs by less than 0.7‰ from values of Fortier and Lüttge (1995) (Fig. 9). Carbonate substituted to channel ions is isotopically heavier than carbonate substituted to phosphate, leading to a higher oxygen intracrystalline isotopic fractionation with phosphate, by ~6‰ at 300 K. Theoretical carbonate – phosphate fractionation in carbonated fluorapatite at 37 °C, 8.47‰, compares with the measurements of Bryant et al. (1996) and Iacumin et al. (1996) on biogenic apatites, 8.56‰ and 8.86‰ respectively. This further sustains the use of the B-type carbonated apatite model investigated in this work as a representative proxy for investigating the isotopic properties of natural B-type carbonate-bearing bio-apatites. Phosphate oxygen isotope ratio is considered less susceptible to diagenetic alteration than carbonate isotope ratio since the oxygen in P–O bonds is very resistant to inorganic isotopic exchange with aqueous fluids (Lécuyer et al., 1999; Sharp et al., 2000; Zazzo et al., 2004b). In contrast, during biologically-mediated reactions, the kinetics of microbially-induced oxygen isotope exchange between phosphate and water is faster than between carbonate and water (Zazzo et al., 2004b). Oxygen isotope fractionation between phosphate and carbonate in apatite is thus thought to be a test for diagenetic alteration (Iacumin et al., 1996; Zazzo et al., 2004a), with samples deviating from the mean carbonate-phosphate fractionation ratio considered to be diagenetically altered. The commonly mean value reported in the literature for carbonate – phosphate fractionation in modern and preserved fossil bio-apatites, $\Delta^{18}O_{C\text{-}P} \sim 9‰$ (Martin et al., 2008), is consistent with the 8.5‰ fractionation factor calculated here at 37 °C between carbonate and phosphate in carbonated fluorapatite. The carbonate-phosphate relationship displays a natural variability (e.g. inter-species differences, inter-laboratory differences) and Pellegrini et al. (2011) advise caution in using a constant offset between carbonate and phosphate, especially when converting bioapatite $\delta^{18}O_C$ to $\delta^{18}O_P$. Indeed, Tutken (2014) found $\Delta^{18}O_{C\text{-}P}$ offsets ranging from 7 to 10‰ in a series of Eocene well-preserved vertebrate fossils. Lécuyer et al. (1999) found a mean $\Delta^{18}O_{C\text{-}P} \sim 8‰$ in a series of recent phosphorites but observed deviations from the mean value with increasing age that could possibly be related to diagenesis.

Carbonate/phosphate fractionation factors calculated from carbonate (Lécuyer et al., 2010) and phosphate (Kolodny et al., 1983) equations at 37 °C and 10 °C imply a stronger temperature dependence of the carbonate/phosphate fractionation than what our calculations suggest for equilibrium fractionation in this temperature range. As discussed above on the basis of mineral-water fractionation curves, this effect could be due to the temperature dependent incorporation of a fraction of carbonate groups in A sites.

4.2. Equilibrium isotopic fractionation of carbon $^{13}C/^{12}C$

High temperature carbon isotope fractionation values between carbon dioxide and calcite can be compared with data from Chacko et al. (1991). The inflexion point of the fractionation curve is calculated at around T = 430 °C. At low temperatures, calculated carbon isotope fractionation factors are higher than experimentally determined values (Romanek et al., 1991) (Fig. 10). Here, it can be noticed that in this specific system, the cross-over between the CO_2 and calcite β-factor curves may amplify the relative discrepancy between theoretical and experimental fractionation factors.

Carbon isotope fractionation between calcite and carbonate-bearing apatite phases is ~4‰ at 300 K. B-type carbonated apatites are depleted in ^{13}C while A-type carbonated apatite is enriched in ^{13}C relative to calcite (Fig. 11). Once again the substitution site for carbonate in apatite affects the isotopic properties of the apatite – calcite system. A major question pertains to the alteration mechanisms of bio-apatite, particularly whether they involve dissolution – recrystallization of biogenic apatites in favour of a phase approaching carbonated fluorapatite or rather leaching of channel ions and their replacement by fluoride (Kolodny et al., 1996; Zazzo et al., 2004a, 2004b; Pasteris and Ying, 2009; Trueman and Tuross, 2002; Kohn, 2008; Kohn and Moses, 2013). Results shown in Fig. 11 suggest that, ionic exchange at A-site and leaching of channel carbonate could deplete apatite in the heavy isotope.

4.3. Equilibrium isotopic fractionation of calcium $^{44}Ca/^{40}Ca$

Calcium isotope fractionation between apatite phases and calcite is very small and falls within 1.5‰ (Fig. 12a). Interestingly, hydroxyapatite and B-type carbonated apatites are depleted in heavy isotope while A-type carbonated apatite is to a small extent enriched in ^{44}Ca relative to calcite. Though Ca is not as closely related to the carbonate group as oxygen and carbon, the substitution site for carbonate in apatite still has an impact on the calcium isotope fractionation properties of apatite. If the equilibrium fractionation between $Ca^{2+}_{(aq)}$ and calcite is almost nil, as suggested by Fantle and DePaolo, 2007, theoretical equilibrium fractionation factors between apatite and calcite should match those of apatite and aqueous calcium. At equilibrium, the fractionation factor between hydroxyapatite and calcite is also weak (−0.17‰ at 37 °C, −0.21‰ at 10 °C). The variability of calcium fractionation factors calculated at T = 37 °C (Table 3) may contribute to the range of $\delta^{44/40}Ca$ measured in vertebrates modern and fossil bio-apatite samples, between +0.7 and −2.7‰ (Gussone et al., 2016). Schmitt et al. (2003) showed similar Ca isotopic trends in Miocene marine calcium phosphates and carbonates with a small positive fractionation between hydroxyapatite and calcite (<0.2‰ for the recent samples). A small magnitude of Ca isotopic fractionation between apatite and calcite is therefore sustained by both theoretical modelling and measurements on natural samples.

Calcium isotope fractionation between hydroxyapatite and $[Ca(H_2O)_6]^{2+}$ is close to zero (Table S4), which differs from the enrichment in ^{44}Ca in phosphates relative to free Ca^{2+}calculated by Moynier and Fujii (2017). The presently calculated fractionation factor between B-type carbonated apatite and $[Ca(H_2O)_6]^{2+}$, −0.78‰ at 37 °C, is consistent

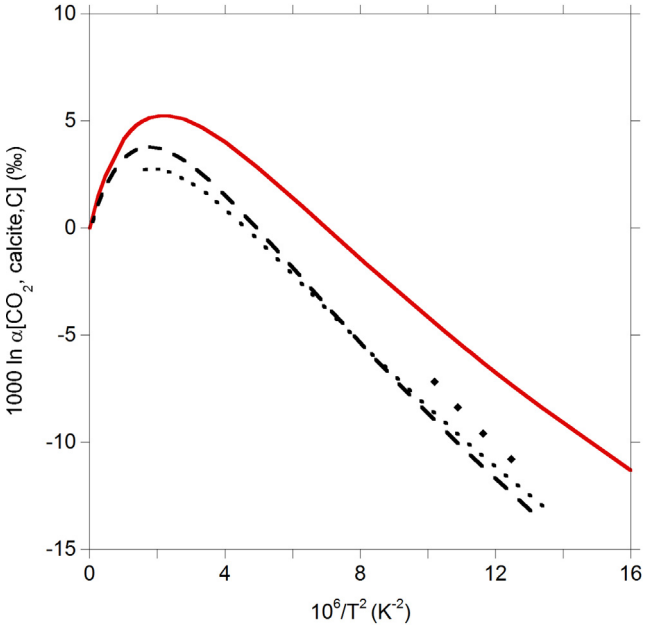

Fig. 10. Theoretical carbon isotope fractionation factor between carbon dioxide and calcite (solid line). Experimental carbon fractionation factors at low temperatures by Romanek et al. (1991) in solid diamonds and calculated carbon isotope fractionation factors from Chacko et al. (1991) (dashed line) and Bottinga (1967) (dotted line).

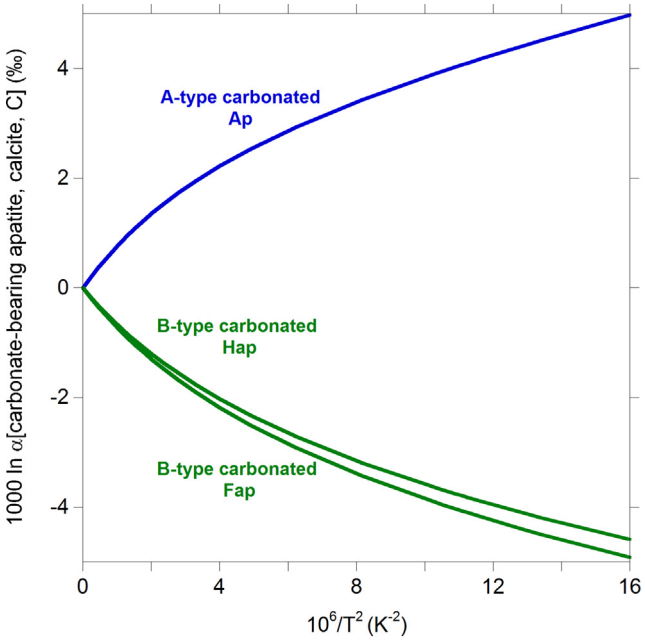

Fig. 11. Theoretical carbon isotope fractionation factor between B-type carbonated fluorapatite, B-type carbonated hydroxyapatite or A-type carbonated apatite and calcite.

with enrichment in ^{44}Ca observed in blood relative to bone, on average ~0.7‰ (Skulan and DePaolo, 1999; Tacail et al., 2014). However, long-range solvation effects and potential contribution of hepta-coordinated Ca species in solution could decrease the reduced partition function ratio of Ca with respect to that of the $[Ca(H_2O)_6]^{2+}$ cluster (Rustad et al., 2010; Moynier and Fujii, 2017). In addition, theoretical results only involve inorganic equilibrium isotopic fractionation and their extrapolation to biological processes involving a complex biomaterial such as bone should be subject to caution. The present results also indicate that long range periodicity should be taken into

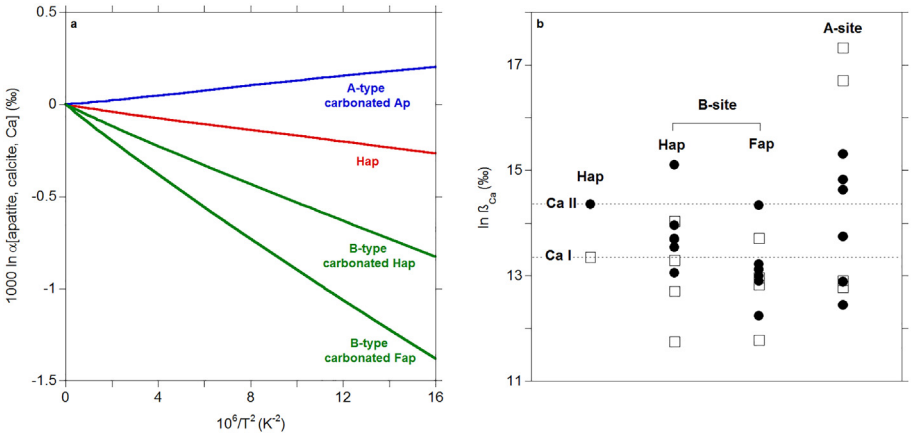

Fig. 12. (a) Theoretical calcium isotope fractionation factor between the various apatite models (hydroxyapatite, B-type carbonated fluorapatite, B-type carbonated hydroxyapatite and A-type carbonated apatite) and calcite. (b) Theoretical calcium β-factor values at 273 K of Ca(I) and Ca(II) sites in hydroxyapatite and for each Ca atom in B-site carbonated hydroxyapatite, B-site carbonated fluorapatite and A-site carbonated apatite.

Table 3
Logarithm of calcium isotope fractionation factors (‰) between hydroxyapatite, B-type carbonated hydroxyapatite, B-type carbonated fluorapatite or A-type carbonated apatite and calcite at T = 37 °C.

	1000 ln α (apatite, calcite, Ca)
Hydroxyapatite	−0.17‰
B-type carbonated hydroxyapatite	−0.55‰
B-type carbonated fluorapatite	−0.93‰
A-type carbonated apatite	+0.14‰

account for the modelling of the isotopic fractionation properties of minerals while the use of clusters could provide a more appropriate description of ionic and molecular structures in solution.

In hydroxyapatite, higher fractionation takes place at the sevenfold coordinated Ca(II) site than at the ninefold coordinated Ca(I) site. This is consistent with the work of Colla et al. (2013) who observed a correlation between calcium isotope fractionation and coordination number between solvated calcium ions and their solid hydrates, concluding that low-coordination environments result in heavier isotopic compositions, in agreement with the general rule of thumb (Schauble, 2004; Blanchard et al., 2017). In the carbonate-bearing models, the presence of the carbonate group affects both the Ca(I) and Ca(II) sites (Fig. 12b). Although the B-type substitution affects the average values of reduced partition function ratio of Ca in the H-apatite model by less than 0.6‰ (Fig. 4b), a site-by-site analysis reveals a range of variation exceeding 3‰. A similar range of variation is observed in the F-bearing model, with a decrease in the reduced partition function ratio of the Ca(II) site reaching 1.25‰. This stronger variation may be due to the presence of two fluorine atoms in the coordination polyhedron of Ca(II) in B-type carbonated fluorapatite. In A-type carbonated apatite, the range of variation of the Ca reduced partition function ratio reaches 4.5‰. This is due to the relatively high values of the reduced partition function ratios (>16.5‰) observed for the two Ca(I) sites not located in the same plane as the C atom (z = 1/2) but on the z = 0 plane. Because of the steric hindrance due to the addition of one oxygen belonging to the carbonate group, the distances between the Ca atom and the oxygen atoms located in the trigonal prism of their ninefold coordination polyhedron are shorter than in pure hydroxyapatite (2.37 Å vs 2.42 Å, respectively). As shorter bonds tend to be stiffer this could favour enrichment in heavy isotopes. Although it is difficult to extract definite trends from the present theoretical results, carbonate substitution in the apatite structure has an effect on the Ca isotopic fractionation properties of apatite and could contribute to the variability measured in natural samples. In any case, the present results suggest that the use of phosphates as a record of seawater Ca isotope composition should be supported by a detailed assessment of their crystal-chemical characteristics to reduce the related variability in isotopic fractionation factors. Rather than dismissing calcium phosphate as a proxy when discrepancies arise, interpreting differences in a multi-proxy approach may actually unravel information about the Ca cycle (Fantle and Tipper, 2014) and encourage to investigate Ca isotopic records in phosphates as well as carbonates.

5. CONCLUSION

In the present study, we have theoretically investigated the equilibrium isotopic fractionation properties of apatite which could help to discuss equilibrium vs. kinetic effect in the record of the isotopic composition associated with processes involving solids and aqueous solutions. The theoretical results revealed differences in oxygen, carbon and calcium isotope fractionation depending on the substitution site for carbonate in apatite. A-type and B-type substitution of carbonates (channel ion substitution and phosphate ion substitution respectively) are distinguishable by their isotopic properties, the A-type carbonate model being comparatively enriched in heavy isotopes (^{18}O, ^{13}C, ^{44}Ca).

Beside the inter-site isotopic fractionation potentially occurring during the formation of minerals, this also demonstrates the importance of investigating site-specific isotopic fractionation alongside substitution and mineral transformation mechanisms (e.g. Putnis, 2009) during diagenesis in order to assess the degree of preservation of the original isotopic signal in apatite, an important limitation for successful paleoenvironmental and paleoclimatic studies based on stable isotope analysis of fossils.

ACKNOWLEDGMENTS

This work was performed using HPC resources from GENCI-IDRIS (Grants i2106041519). This work was supported by French state funds within the framework of the Cluster of Excellence MATISSE led by Sorbonne Universités and also by CNRS TelluS INSU 2017 INTERRVIE. We thank three anonymous reviewers and associate editor Ruth E. Blake for their thoughtful comments.

APPENDIX A. SUPPLEMENTARY MATERIAL

Supplementary data associated with this article can be found, in the online version, at https://doi.org/10.1016/j.gca.2017.09.020.

REFERENCES

Arning E., Lückge A., Breuer C., Gussone N., Birgel D. and Peckmann J. (2009) Genesis of phosphorite crusts off Peru. *Mar. Geol.* **262**, 68–81.

Balan E., Lazzeri M., Delattre S., Méheut M., Refson K. and Winkler B. (2007) Anharmonicity of inner OH-stretching modes in hydrous phyllosilicates: assessment from first-principles frozen phonon calculations. *Phys. Chem. Miner.* **34**, 621–625.

Balan E., Delattre S., Roche D., Segalen L., Morin G., Guillaumet M., Blanchard M., Lazzeri M., Brouder C. and Salje E. K. H. (2011) Line-broadening effects in the powder infrared spectrum of apatite. *Phys. Chem. Miner.* **38**, 111–122.

Baroni S., de Gironcoli S. and Corso A. D. (2001) Phonons and related crystal properties from density- functional theory. *Rev. Mod. Phys.* **73**, 515–562.

Bigeleisen J. and Mayer M. G. (1947) Calculation of equilibrium constants for isotopic exchange reactions. *J. Chem. Phys.* **15**(5), 261–267.

Blake R. E., O'Neil J. R. and Surkov A. V. (2005) Biogeochemical cycling of phosphorus: Insights from oxygen isotope effects of phosphoenzymes. *Am. J. Sci.* **305**, 596–620.

Blanchard M., Balan E. and Schauble E. (2017) Equilibrium fractionation of non-traditional isotopes; a molecular modelling perspective. *Rev. Mineral. Geochem.* **82**, 27–63.

Bottinga Y. (1967) Calculations of fractionation factors for carbon and oxygen isotopic exchange in the system calcite-carbon dioxide-water. *J. Phys. Chem.* **72**, 800–808.

Bottinga Y. and Craig H. (1969) Oxygen isotope fractionation between CO_2 and water, and the isotopic composition of marine atmospheric CO_2. *Earth Planet. Sci. Lett.* **5**, 285–295.

Bryant J. D., Koch P. L., Froelich P. N., Showers W. J. and Genna B. J. (1996) Oxygen isotope partitioning between phosphate and carbonate in mammalian apatite. *Geochim. Cosmochim. Acta* **60**, 5145–5148.

Chacko T., Mayeda T. K., Clayton R. N. and Goldsmith J. R. (1991) Oxygen and carbon isotope fractionations between CO_2 and calcite. *Geochim. Cosmochim. Acta* **55**, 2867–2882.

Chacko T., Cole D. R. and Horita J. (2001) Equilibrium oxygen, hydrogen and carbon isotope fractionation factors applicable to geologic systems. In *Stable Isotope Geochemistry*, vol. 43 (eds. J. W. Valley and D. R. Cole). Mineralogical Society of America, Chantilly, Virginia, pp. 1–62.

Chadi D. J. and Cohen M. L. (1973) Special points in the Brillouin Zone. *Phys. Rev. B* **8**, 5747–5753.

Chang S. J. and Blake R. E. (2015) Precise calibration of equilibrium oxygen isotope fractionations between dissolved phosphate and water from 3 to 37 °C. *Geochim. Cosmochim. Acta* **150**, 314–329.

Colla C. A., Wipenny J., Yin Q.-Z., Rustad J. R. and Casey W. H. (2013) Calcium isotope fractionation between solution and solids with six, seven or eight oxygens bound to Ca(II). *Geochim. Cosmochim. Acta* **121**, 363–373.

De La Rocha C. L. and DePaolo D. J. (2000) Isotopic evidence for variations in the marine calcium cycle over the Cenozoic. *Science* **289**, 1176–1178.

Dupuis R., Benior M., Nardin E. and Méheut M. (2015) Fractionation of silicon isotopes in liquids: the importance of configurational disorder. *Chem. Geol.* **396**, 239–254.

Elliott J. C. (2002) Calcium phosphate biominerals. In *Phosphates-Geochemical, Geobiological and Materials Importance*, vol. 48 (eds. M. J. Kohn, J. Rakovan and J. M. Hughes). Mineralogical Society of America, Chantilly, Virginia, pp. 427–453.

Fantle M. S. and DePaolo D. J. (2007) Ca isotopes in carbonate sediment and pore fluids from ODP Site 807A: the $Ca^{2+}_{(aq)}$-calcite equilibrium fractionation factor and calcite recrystallization rates in Pleistocene sediments. *Geochem. Cosmochem. Acta* **71**, 2524–2546.

Fantle M. S. and Tipper E. T. (2014) Calcium isotopes in the global biogeochemical Ca cycle: implications for the development of a Ca isotope proxy. *Earth Sci. Rev.* **129**, 148–177.

Farkas J., Böhm F., Wallmann K., Blenkisop J., Eisenhauer A., van Geldern R., Munnecke A., Voigt S. and Veizer J. (2007). *Geochem. Cosmochem. Acta* **71**, 5117–5134.

Favot F. and Dal Corso A. (1999) Phonon dispersions: performance of the generalized gradient approximation. *Phys. Rev. B* **60**(16), 427–431.

Fleet M. E. (2009) Infrared spectra of carbonate apatites: ν_2-region bands. *Biomaterials* **30**, 1473–1481.

Fortier S. M. and Lüttge A. (1995) An experimental calibration of the temperature dependence of oxygen isotope fractionation between apatite and calcite at high temperatures (350–800 °C). *Chem. Geol.* **125**, 281–290.

Gehler A., Tütken T. and Pack A. (2011) Triple oxygen isotope analysis of bioapatite as tracer for diagenetic alteration of bones and teeth. *Palaeogeogr. Palaeoclimatol. Palaeoecol.* **210**, 84–91.

Giannozzi P. et al. (2009) Quantum ESPRESSO: a modular and open-source software project for quantum simulations of materials. *J. Phys.: Condens. Matter* **21**, 395502.

Graf D. L. (1961) Crystallographic tables for the rhombohedral carbonates. *Am. Miner.* **46**, 1283–1316.

Griffith E. M., Schauble E. A., Bullen T. D. and Paytan A. (2008) Characterization of calcium isotopes in natural and synthetic barite. *Geochim. Cosmochim. Acta* **72**, 5641–5658.

Gussone N., Böhm F., Eisenhauer A., Dietzel M., Heuser A., Teichert B. M. A., Reitner J., Wörheide G. and Dullo W.-C. (2005) Calcium isotope fractionation in calcite and aragonite. *Geochim. Cosmochim. Acta* **69**, 4485–4494.

Gussone N., Schmitt A.-D., Heuser A., Wombacher F., Dietzel M., Tipper E. and Schiller M. (2016) *Calcium Stable Isotope Geochemistry*. Springer, Berlin Heidelberg, p. 260.

Hamann D. R. (2013) Optimized norm-conserving Vanderbilt pseudopotentials. *Phys. Rev. B* **88**, 085117.

Heuser A., Eisenhauer A., Böhm F., Wallmann K., Gussone N., Pearson P. N., Nägler T. F. and Dullo W.-C. (2005) Calcium isotope ($\delta^{44}/^{40}$Ca) variations of Neogene planktonic foraminifera. *Paleoceanography* **20**, PA2013. https://doi.org/10.1029/2004PA001048.

Heuser A., Tütken T. and Galer S. J. G. (2009) Calcium isotope systematics of dinosaur teeth. *Geochim. Cosmochim. Acta* **73** (Suppl. 1), A528.

Heuser A., Tütken T., Gussone N. and Galer S. J. G. (2011) Calcium isotopes in fossil bones and teeth – diagenetic versus biogenic origin. *Geochim. Cosmochim. Acta* **75**, 3419–3433.

Hohenberg P. and Kohn W. (1964) Inhomogeneous electron gas. *Phys. Rev.* **136**, 864–871.

Horita J. and Wesolowski D. J. (1994) Liquid-vapor fractionation of oxygen and hydrogen isotopes of water from the freezing to the critical temperature. *Geochim. Cosmochim. Acta* **58**, 3425–3437.

Hughes J. M., Cameron M. and Crowley K. D. (1989) Structural variations in natural F, OH and Cl apatites. *Am. Miner.* **74**, 870–876.

Hughes J. M., Cameron M. and Crowley K. D. (1990) Crystal structures of natural ternary apatites: solid solution in the $Ca_5(PO_4)_3X$ (X = F, OH, Cl) system. *Am. Miner.* **75**, 295–304.

Iacumin P., Bocherens H., Mariotti A. and Longinelli A. (1996) Oxygen isotope analyses of co-existing carbonate and phosphate in biogenic apatite: a way to monitor diagenetic alteration of bone phosphate? *Earth Planet Sci. Lett.* **142**, 1–6.

Kim S.-T. and O'Neil J. R. (1997) Equilibrium and nonequilibrium oxygen isotope effects in synthetic carbonates. *Geochim. Cosmochim. Acta* **61**, 3461–3475.

Knudsen A. C. and Gunter M. E. (2002) Sedimentary phosphates – an example: phosphoria formation, Southern Idaho USA. In *Phosphates – Geochemical, Geobiolo Gical and Materials Importance*, vol. 48 (eds. M. L. Kohn, J. Rakovan and J. M. Hughes). Mineralogical Society of America, Chantilly, Virginia, pp. 363–390.

Kohn M. J., Schoeninger M. J. and Valley J. W. (1996) Herbivore tooth oxygen compositions: effects of diet and physiology. *Geochim. Cosmochim. Acta* **60**, 3889–3896.

Kohn M. J. and Cerling T. E. (2002) Stable isotope compositions of biological apatite. In *Phosphates – Geochemical, geobiological and materials importance*, vol. 48 (eds. M. L. Kohn, J. Rakovan and J. M. Hughes). Mineralogical Society of America, Chantilly, Virginia, pp. 455–488.

Kohn M. J. (2008) Models of diffusion-limited uptake of trace elements in fossils and rates of fossilization. *Geochim. Cosmochim. Acta* **72**, 3758–3770.

Kohn M. J. and Moses R. J. (2013) Trace element diffusivities in bone rule out simple diffusive uptake during fossilization but explain in vivo uptake and release. *Proc. Natl. Acad. Sci.* **110**, 419–424.

Kohn W. and Sham L. (1965) Self-consistent equations including exchange and correlation effects. *Phys. Rev.* **140**, A1133–A1138.

Kolodny Y., Luz B. and Navon O. (1983) Oxygen isotope variations in phosphate of biogenic apatites: I. Fish bone apatite – rechecking the rules of the game. *Earth Planet. Sci. Lett.* **64**, 398–404.

Kolodny Y., Luz B., Sander M. and Clemens W. A. (1996) Dinosaur bones: fossils or pseudomorphs? The pitfalls of physiology reconstruction from apatitic fossils. *Palaeogeogr. Palaeoclimatol. Palaeoecol.* **126**, 161–171.

Lécuyer C., Grandjean P. and Sheppard S. M. F. (1999) Oxygen isotope exchange between dissolved phosphate and water at temperatures ≤135°C: inorganic versus biological fractionations. *Geochim. Cosmochim. Acta* **63**, 855–862.

Lécuyer C., Balter V., Martineau F., Fourel F., Bernard A., Amiot R., Gardien V., Otero O., Legendre S., Panczer G., Simon L. and Martini R. (2010) Oxygen isotope fractionation between apatite-bound carbonate and water determined from controlled experiments with synthetic apatites precipitated at 10–37 °C. *Geochim. Cosmochim. Acta* **74**, 2072–2081.

Lee-Thorp J. A. and van der Merwe N. J. (1987) Carbon isotope analysis of fossil bone apatite. *S. Afr. J. Sci.* **83**, 712–715.

Lemarchand D., Wasserburg G. J. and Papanastassiou D. A. (2004) Rate-controlled calcium isotope fractionation in synthetic calcite. *Geochim. Cosmochim. Acta* **68**, 4665–4678.

Liang Y. and Blake R. E. (2007) Oxygen isotope fractionation between apatite and aqueous-phase phosphate: 20–45 °C. *Chem. Geol.* **238**, 121–133.

Longinelli A. (1965) Oxygen isotopic composition of orthophosphate from shells of living marine organisms. *Nature* **207**, 716–719.

Longinelli A. (1984) Oxygen isotopes in mammal bone phosphate: a new tool for paleohydrological and paleoclimatological research? *Geochim. Cosmochim. Acta* **48**, 385–390.

Marriott C. S., Henderson G. M., Belshaw N. S. and Tudhope A. W. (2004) Temperature dependence of δ^7Li, δ^{44}Ca, and Li/Ca during growth of calcium carbonate. *Earth Planet. Sci. Lett.* **222**, 615–624.

Martin C., Bentaleb I., Kaandorp Iacumin P. and Chatri K. (2008) Intra-tooth study of modern rhinoceros enamel δ^{18}O: Is the difference between phosphate and carbonate δ^{18}O a sound diagenetic test? *Palaeogeogr. Palaeoclimatol. Palaeoecol.* **266**, 183–189.

McConell D. (1973) *Apatite, Its Crystal Chemistry, Mineralogy, and Geological and Biological Occurrences*. Springer, NewYork, p. 111p.

Méheut M., Lazzeri M., Balan E. and Mauri F. (2007) Equilibrium isotopic fractionation in the kaolinite, quartz, water system: prediction from first principles density-functional theory. *Geochim. Cosmochim. Acta* **71**, 3170–3181.

Méheut M., Lazzeri M., Balan E. and Mauri F. (2009) Structural control over equilibrium silicon and oxygen isotopic fractionation: a first-principles density-functional theory study. *Chem. Geol.* **258**, 28–37.

Monkhorst H. J. and Pack J. D. (1976) Special points for Brillouin-zone integrations. *Phys. Rev. B* **13**, 5188–5192.

Moynier F. and Fujii T. (2017) Calcium isotope fractionation between aqueous compounds relevant to low-temperature geochemistry, biology and medicine. *Sci. Rep.* **7**, 44255.

Pack A., Gehler A. and Süssenberger A. (2013) Exploring the usability of isotopically anomalous oxygen in bones and teeth as paleo-CO_2-barometer. *Geochim. Cosmochim. Acta* **102**, 306–317.

Pasteris J. D. and Ying D. Y. (2009) Experimental fluoridation of nanocrystalline apatite. *Am. Miner.* **94**, 53–63.

Passey B. H., Hu H., Ji H., Montanari S., Li S., Henkes G. A. and Levin N. E. (2014) Triple oxygen isotopes in biogenic and sedimentary carbonates. *Geochim. Cosmochim. Acta* **141**, 1–25.

Pellegrini M., Lee-thorp J. A. and Donahue R. E. (2011) Exploring the variation of the $\delta^{18}O_p$ and $\delta^{18}O_c$ relations in enamel increments. *Palaeogeogr. Palaeoclimatol. Palaeoecol.* **310**, 71–83.

Perdew J. P., Burke K. and Ernzerhof M. (1996) Generalized gradient approximation made simple. *Phys. Rev. Lett.* **77**, 3865–3868.

Pinilla C., Blanchard M., Balan E., Ferlat G., Vuilleumier R. and Mauri F. (2014) Equilibrium fractionation of H and O isotopes in water from path integral molecular dynamics. *Geochim. Cosmochim. Acta* **135**, 203–216.

Pucéat E., Joachimski M. M., Bouilloux A., Monna F., Bonin A., Motreuil S., Morinière P., Hénard S., Mourin J., Dera G. and Quesne D. (2010) Revised phosphate-water fractionation equation reassessing paleotemperatures derived from biogenic apatite. *Earth Planet. Sci. Lett.* **298**, 135–142.

Putnis A. (2009) Mineral replacement reactions. *Rev. Mineral. Geochem.* **70**, 87–124.

Quade J., Cerling T. E., Barry J. C., Morgan M. E., Pilbeam D. R., Chivas A. R., Lee-Thorp J. A. and van der Merwe N. J. (1992) A 16-Ma record of paleodiet using carbon and oxygen isotopes in fossils teeth from Pakistan. *Chem. Geol.* **94**, 183–192.

Rakovan J. F. and Pasteris J. D. (2015) A technological gem: materials, medical, and environmental mineralogy of apatite. *Elements* **11**, 195–200.

Redlich (1935). *Z. Phys. Chem. B* **28**, 371.

Regnier P., Lasaga A. C., Berner R. A., Han O. H. and Zilm K. W. (1994) Mechanism of CO_3^{2-} substitution in carbonate-fluorapatite: evidence from FTIR spectroscopy, ^{13}C NMR, and quantum mechanical calculation. *Am. Miner.* **79**, 809–818.

Reynard L. M., Henderson G. M. and Hedges R. E. M. (2010) Calcium isotope ratios in animal and human bone. *Geochim. Cosmochim. Acta* **74**, 3735–3750.

Reynard B. and Balter V. (2014) Trace elements and their isotopes in bones and teeth: diet, environments, diagenesis, and dating of archaeological and paleontological samples. *Palaeogeogr. Palaeoclimatol. Palaeoecol.* **416**, 4–16.

Richet P., Bottinga Y. and Javoy M. (1977) A review of hydrogen, carbon, nitrogen, oxygen, sulphur, and chlorine stable isotope fractionation among gaseous molecules. *Annu. Rev. Earth Planet. Sci.* **5**, 65–110.

Roche D., Ségalen L., Balan E. and Delattre S. (2010) Preservation assessment of Miocene-Pliocene tooth enamel from Tugen Hills (Kenyan Rift Valley) through FTIR, chemical and stable-isotope analyses. *J. Archaeol. Sci.* **37**, 1690–1699.

Roche D., Ségalen L., Senut B. and Pickford M. (2013) Stable isotope analyses of tooth enamel carbonate of large herbivores from the Tugen Hills deposits: environmental context of the earliest Kenyan hominids. *Earth Planet. Sci. Lett.* **381**, 39–51.

Romanek C. S., Grossman E. L. and Morse J. W. (1991) Carbon isotopic fractionation in synthetic aragonite and calcite: effects of temperature and precipitation rate. *Geochim. Cosmochim. Acta* **56**, 419–430.

Rustad J. R. and Zarzycki P. (2008) Calculation of site-specific carbon-isotope fractionation in pedogenic oxide minerals. *Proc. Natl. Acad. Sci.* **105**, 10297–10301.

Rustad J. R., Casey W. H., Yin Q.-Z., Bylaska E. J., Felmy A. R., Bogatko S. A., Jackson V. E. and Dixon D. A. (2010) Isotopic fractionation of Mg^{2+}(aq), Ca^{2+}(aq), and Fe^{2+}(aq) with carbonate minerals. *Geochim. Cosmochim. Acta* **74**, 6301–6323.

Schauble E. A. (2004) Applying stable isotope fractionation theory to new systems. In *Geochemistry of Non-traditional Stable Isotopes*, 65 (eds. C. M. Johnson, B. L. Beard and F. Albarède). Mineralogical Society of America, Washington, p. 65.

Schauble E. A., Ghosh P. and Eiler J. M. (2006) Preferential formation of ^{13}C–^{18}O bonds in carbonate minerals, estimated using first-principles lattice dynamics. *Geochim. Cosmochim. Acta* **70**, 2510–2529.

Schmitt A.-D., Stille P. and Vennemann T. (2003) Variations of the $^{44}Ca/^{40}Ca$ ratio in seawater during the past 24 million years: evidence from $\delta^{44}Ca$ and $\delta^{18}O$ values of Miocene phosphates. *Geochim. Cosmochim. Acta* **67**, 2607–2614.

Sharp Z. D., Atudorei V. and Furrer H. (2000) The effect of diagenesis on oxygen isotope ratios of biogenic phosphates. *Am. J. Sci.* **300**, 222.

Skulan J., DePaolo D. J. and Owens T. L. (1997) Biological control of calcium isotopic abundances in the global calcium cycle. *Geochim. Cosmochim. Acta* **61**, 2505–2510.

Skulan J. and DePaolo D. J. (1999) Calcium isotope fractionation between soft and mineralized tissues as a monitor of calcium use in vertebrates. *Proc. Nat. Acad. Sci.* **96**, 13709–13713.

Soudry D., Segal I., Nathan Y., Glenn C. R., Halizc L., Lewy Z. and VonderHaar D. L. (2004) $^{44}Ca/^{42}Ca$ and $^{143}Nd/^{144}Nd$ isotope variations in Cretaceous-Eocene Tethyan francolites and their bearing on phosphogenesis in the southern Tethys. *Geology* **32**, 389–392.

Soudry D., Glenn C. R., Nathan Y., Segal I. and VonderHaar D. L. (2006) Evolution of Tethyan phosphogenesis along the northern edges of the Arabian-African shield during the Cretaceous-Eocene as deduced from temporal variations of Ca and Nd isotopes and rates of P accumulation. *Earth Sci. Rev.* **78**, 27–57.

Stolper D. A. and Eiler J. M. (2015) The kinetics of solid-state isotope exchange reactions for clumped isotopes: a study of inorganic calcites and apatites from natural and experimental samples. *Am. J. Sci.* **315**, 363–411.

Tacail T., Albalat E., Télouk P. and Balter V. (2014) A simplified protocol for measurement of Ca isotopes in biological samples. *J. Anal. At. Spectrom.* **29**, 529–535.

Tacail T., Télouk P. and Balter V. (2016) Precise analysis of calcium stable isotope variations in biological apatites using laser ablation MC-ICPMS. *J. Anal. At. Spectrom.* **31**, 152–162.

Trueman C. N. and Tuross N. (2002) Trace elements in recent fossil bone apatite. *Rev. Mineral. Geochem.* **48**, 489–521.

Tutken T. (2014) Isotope compositions (C, O, Sr, Nd) of vertebrate fossils from the Middle Eocene oil shale of Messel, Germany: implications for their taphonomy and palaeoenvironment. *Palaeogeogr. Palaeoclimatol. Palaeoecol.* **416**, 92–109.

Wacker U., Rutz T., Löffler N., Conrad A. C., Tütken T., Böttcher M. E. and Fiebig J. (2016) Clumped isotope thermometry of carbonate-bearing apatite: revised sample pre-treatment, acid digestion, and temperature calibration. *Chem. Geol.* **443**, 97–110.

Wang W., Qin T., Zhou C., Huang S., Wu Z. and Huang F. (2017) Concentration effect on equilibrium fractionation of Mg-Ca isotopes in carbonate minerals: insights from first-principles calculations. *Geochim. Cosmochim. Acta* **208**, 185–197.

Yi H., Balan E., Gervais C., Segalen L., Fayon F., Roche D., Person A., Morin G., Guillaumet M., Blanchard M., Lazzeri M. and Babonneau F. (2013) A carbonate-fluoride defect model for carbonate-rich fluorapatite. *Am. Miner.* **98**, 1066–1069.

Yi H., Balan E., Gervais C., Ségalen L., Blanchard M. and Lazzeri M. (2014a) Theoretical study of the local charge compensation and spectroscopic properties of B-type carbonate defects in apatite. *Phys. Chem. Miner.* **41**, 347–359.

Yi H., Balan E., Gervais C., Ségalen L., Roche D., Person A., Fayon F., Morin G. and Babonneau F. (2014b) Probing atomic scale transformation of fossil dental enamel using Fourier transform infrared and nuclear resonance magnetic spectroscopy: a case from the Tugen Hills (Rift Gregory, Kenya). *Acta Biomater.* **10**, 3952–3958.

Young E. D., Galy A. and Nagahara H. (2002) Kinetic and equilibrium mass-dependent isotope fractionation laws in nature and their geochemical and cosmochemical significance. *Geochim. Cosmochim. Acta* **66**, 1691–1698.

Zazzo A., Lécuyer C. and Mariotti A. (2004a) Experimentally-controlled carbon and oxygen isotope exchange between

bioapatites and water under organic and microbially-mediated conditions. *Geochim. Cosmochim. Acta* **68**, 1–12.

Zazzo A., Lécuyer C., Sheppard S. M. F., Grandjean P. and Mariotti A. (2004b) Diagenesis and the reconstruction of paleoenvironments: a method to restore original $\delta^{18}O$ values of carbonate and phosphate from fossil tooth enamel. *Geochimica et Cosmochimica Acta* **68**, 2245–2258.

Zheng Y.-F. (2016) Oxygen isotope fractionation in phosphates: the role of dissolved complex anions in isotope exchange. *Isot. Environ. Health Stud.* **52**, 47–60.

Associate editor: Ruth Blake